Journal of Engineering Science *Vol. XXX, no. 4 (2023), pp. 45 - 62*
Fascicle *Electronics and Computer Science* *ISSN 2587-3474*
Topic *Microelectronics and Nanotechnologies* *eISSN 2587-3482*

https://doi.org/10.52326/jes.utm.2023.30(4).04
UDC 620.3:621.315.55

ANNEALING EFFECT ON UV DETECTION PROPERTIES OF ZnO:Al STRUCTURES

Rajat Nagpal [1], ORCID: 0009-0007-1266-1892,
Maxim Chiriac [1], ORCID: 0000-0003-2163-8735,
Alexandr Sereacov [1], ORCID: 0009-0002-7060-5227,
Adrian Birnaz [1], ORCID: 0000-0002-2906-7255,
Nicolai Ababii [1], ORCID: 0000-0001-5046-8611,
Cristian Lupan [1], ORCID: 0000-0003-2268-6181,
Artur Buzdugan [1], ORCID: 0000-0002-9226-004X,
Iulia Sandu [1], ORCID: 0009-0001-7213-8290,
Leonard Siebert [2], ORCID: 0000-0001-5316-7240,
Thierry Pauporté [3], ORCID: 0000-0001-5906-8075,
Oleg Lupan [1,2,3,4*], ORCID: 0000-0002-7913-9712

[1] *Technical University of Moldova, 168 Stefan cel Mare Blvd., Chisinau, Republic of Moldova*
[2] *Kiel University, Kaiserstr. 2, D-24143, Kiel, Germany*
[3] *PSL University, Institut de Recherche de Chimie Paris-IRCP, CNRS – Chimie ParisTech, 75231 Paris Cedex 05, France*
[4] *University of Central Florida, Orlando, FL 32816-2385, USA*
*Corresponding author: Oleg Lupan, *oleg.lupan@mib.utm.md*

Received: 12. 04. 2023
Accepted: 12. 22. 2023

Abstract. The aim of this study was to develop low-powered, highly selective UV sensor to continuously monitor personalized UV exposure as well as to study annealing effect on UV detection properties of the sensors. ZnO:Al structures were obtained by chemical growth method followed by thermal annealing at 625 °C for 2 h. The studied samples exhibit maximal UV response of 620/488 at 25 °C/50 °C to 370 nm UV radiation before/after annealing, respectively. Thermal annealing of sensor (250 °C for 1 h) led to improvement in fall time from 3860 seconds to 262 seconds at 25 °C and highest responsivity (~48 mA/W) came out for 370 nm wavelength at 75 °C operating temperatures. Consequently, excellent selectivity for 370 nm UV illumination can be ascribed as due to thermal annealing effect which increases the crystallinity, grain size, and roughness of the sensing film. The PL measurements reveals the suppression of structural defects, increase in intensity after annealing and enhanced UV response due to presence of Al content in films. Overall, these structures showed magnificent UV properties, before and especially after additional thermal annealing. UV sensing mechanism of such nanomaterial-based sensor were explained with physio-chemical processes take place on the surface of these structures. The obtained results on annealed ZnO:Al films-based devices is superior to reported performances of other nanostructures, proving new results for UV sensing applications at different operating temperatures in various fields.

Keywords: *semiconductor oxide, heterostructure, sensor, selectivity, efficiency, sensing mechanism.*

Rezumat. Scopul acestui studiu a fost de a dezvolta un senzor UV de putere redusă, foarte selectiv, pentru a monitoriza continuu expunerea personalizată la UV, precum și pentru a studia efectul de recoacere asupra proprietăților de detectare UV a senzorilor. Structurile ZnO:Al au fost obținute prin metoda de creștere chimică urmată de recoacere termică la 625 °C timp de 2 ore. Probele studiate prezintă un răspuns UV maxim de 620/488 la 25 °C/50 °C până la 370 nm radiații UV înainte/după recoacere, respectiv. Recoacere termică a senzorului (250 °C timp de 1 oră) a condus la îmbunătățirea timpului de cădere de la 3860 de secunde la 262 de secunde la 25 °C și cea mai mare capacitate de răspuns (~48 mA/W) a rezultat pentru o lungime de undă de 370 nm la temperaturi de funcționare de 75 °C. În consecință, selectivitatea excelentă pentru iluminarea UV de 370 nm poate fi atribuită ca fiind datorată efectului de recoacere termică care crește cristalinitatea, dimensiunea granulelor și rugozitatea filmului de detectare. Măsurătorile PL relevă suprimarea defectelor structurale, creșterea intensității după recoacere și răspunsul UV îmbunătățit datorită prezenței conținutului de Al în pelicule. În general, aceste structuri au arătat proprietăți UV magnifice, înainte și mai ales după recoacere termică suplimentară. Mecanismul de detectare UV al unui astfel de senzor pe bază de nanomateriale a fost explicat cu procesele fizico-chimice care au loc pe suprafața acestor structuri. Rezultatele obținute pe dispozitivele pe bază de filme recoapte ZnO:Al sunt superioare performanțelor raportate ale altor nanostructuri, dovedind rezultate noi pentru aplicațiile de detectare UV la diferite temperaturi de funcționare în diferite domenii.

Cuvinte cheie: *oxid semiconductor, heterostructură, senzor, selectivitate, eficiență, mecanism de detectare.*

1. Introduction

Radiation in ultraviolet spectrum plays a crucial role in our daily life. We can observe its distinct outcomes, even if we do not visualize it with naked eye. We find enormous applications of distinct ultraviolet (UV) radiations in domestic and industrial fields, but we also get affected by its over exposure. Ultraviolet (UV) light can adversely affect human body especially eyes, and special lenses are used with a wavelength filter in the ultraviolet range 400 – 450 nm to minimize UV influence on it [1]. Kraemer et al. demonstrated effect of UV light small group of people with basal cell nevus syndrome and other skin disorders which may cause skin cancer [2]. Ultraviolet light source provides efficient light used in several areas such as: creating integrated circuits [3]; medicine [4–7]; food industry [8,9]; agriculture [10]; cosmetics [11,12]; personalized sensors [13], etc. In integrated circuits, UV light cures light–sensitive materials, e.g., photoresist as a substrate [3]. In the field of dental medicine, ultraviolet is used to cure biocompatible polymers for the restoration of fractured teeth [4]. Additionally, UV light is used on the skin to reduce inflammation and trigger biological processes in dermatology in so-called phototherapy [7]. Another application of ultraviolet light in medicine is for disinfection, e.g., during the SARS-CoV-2 period rooms were systematically illuminated with the aim of decontamination [5]. In food industry, UV light is used instead of thermal treatment of liquids, so the pasteurization process is no longer necessary [8]. Agriculture is still influenced by UV irradiations significantly with positive effects. Recent studies have shown that short-term exposure of plants to ultraviolet radiation positively influences the exposed plant by increasing the levels of bioactive substances [10].

Devices with UV light-emitting diodes (LEDs) are used in cosmetics to cure nail polish. These devices are easily accessible in domestic conditions, but at the same time raise possible complications to patients in dermatology and ophthalmology [11]. Different substances used in cosmetics are also being studied to filter ultraviolet rays coming from the sun [12]. The purpose of UV sensors is to continuously monitor exposure time of human body to ultraviolet rays [13]. Of course, the ultraviolet rays that are emitted by the sun are essential for the human body to synthesize vitamin D which itself is necessary for muscle health, but excessive exposure to these rays can lead to various aggravations. The main adverse consequences are cutaneous malignant melanoma, squamous cell carcinoma of the skin or basal cell carcinoma of the skin [14]. In addition, the skin loses its elasticity, ages faster and can develop solar keratoses. There are also serious effects of UV radiation on the eyes such as cataracts, which can cause various complications such as complete loss of vision as well as pterygium. So, the applications of UV radiation require rigorous control, especially in areas related to human health.

Wide-bandgap metal oxide semiconductors have been shown to be high-performance UV photodetectors with promising photo responsivities compared to commercial devices. ZnO is preferred among these materials for use in UV photodetector because it possesses a wide direct band gap (~3.37 eV) corresponding to the energy of an ultraviolet photon, native *n*-type conductivity, and high exciton binding energy (60 meV) at room temperature, which are properties unique and attractive for UV photodetection. Besides these, ZnO can be obtained by various technologies, and especially attractive structured nanomaterials, which open new promising applications. Altering the band gap energy of the sensing structure by doping of is necessary to adjust the sensing range and improve the selectivity for a given UV illumination spectrum [15,16]. Aluminum is frequently used to achieve better optical and electrical properties of ZnO by replacing Zn^{2+} ions with Al^{3+}. Azizah et al. demonstrated [17] that apposite Al doping may increase the energy of the band gap and illustrated that the Al doping enhances photo to dark current ratio. The increase in the ZnO band gap may be due to the occupation of the lowest levels in the conduction band by the electrons of the Al impurity atoms which causes a direct transition with higher energy. The optical band gap values were those obtained by room temperature photoluminescence spectra in ZnO and ZnO:Al [18]. An illustrated example shows doping of ZnO with 3% Al allows the expansion of band gap from 3.37 eV to 3.9 eV and the increase of the electron density of electrons by about 5 times (up to $4.5 \cdot 10^{20}$ cm^{-3}). Hence, Al-doping improves photosensitivity of ZnO. Most of the studies based on ZnO:Al photodetection illustrates sensing at relatively high bias voltages, e.g. at about 5 V. Therefore, it is the high interest to investigate effect of annealing on the UV detection performances of aluminum-doped ZnO films.

Our current study showed an excellent ZnO:Al structures exhibiting decrease in photo current fall rate at low bias voltage of 1 V with excellent rejection ratio of >20 times to other interfering wavelengths i.e., 385 nm and 394 nm after thermal annealing. Ultraviolet spectrum with diverse applications shows bittersweet character, so it is necessary to develop personalized sensors for determining the exposure of different surfaces to UV inclusively and determining the wavelength that is applied at the time of the actual exposure. In this work structural properties of ZnO:Al depositions are studied with its UV sensory properties at three UV wavelengths in different operating conditions and annealing effect.

2. Materials and Methods

The ZnO:Al structures have been obtained by the chemical method, which is easy to achieve and effective from the point of view of costs [19], followed by thermal annealing at 625°C for 2 hours [20], techniques presented in detail previously [19,21,22]. Thermal annealing improves the crystal quality of thin films synthesized in chemical solutions [21–23] by densifying them compared to those obtained at room temperature.

The structural, morphological, photoluminescence and micro-Raman studies were analyzed and discussed in detail. For measurement of XRD, graphite monochromatized $CuK_{\alpha 1}$ radiation with wavelength as λ =1.5405 Å using Siefert 3000TT unit at 40 mA and 40 kV.

UV Installation

Schematic setup of the measuring installation shown in Figure 1. The measuring installation consists of the following discrete modules: LEDs of different wavelengths are placed on a round aluminum printed circuit board in the UV diapason. This printed circuit board is rotated by a stepper motor, ensuring that the emitting LED is placed exactly on the sample under study.

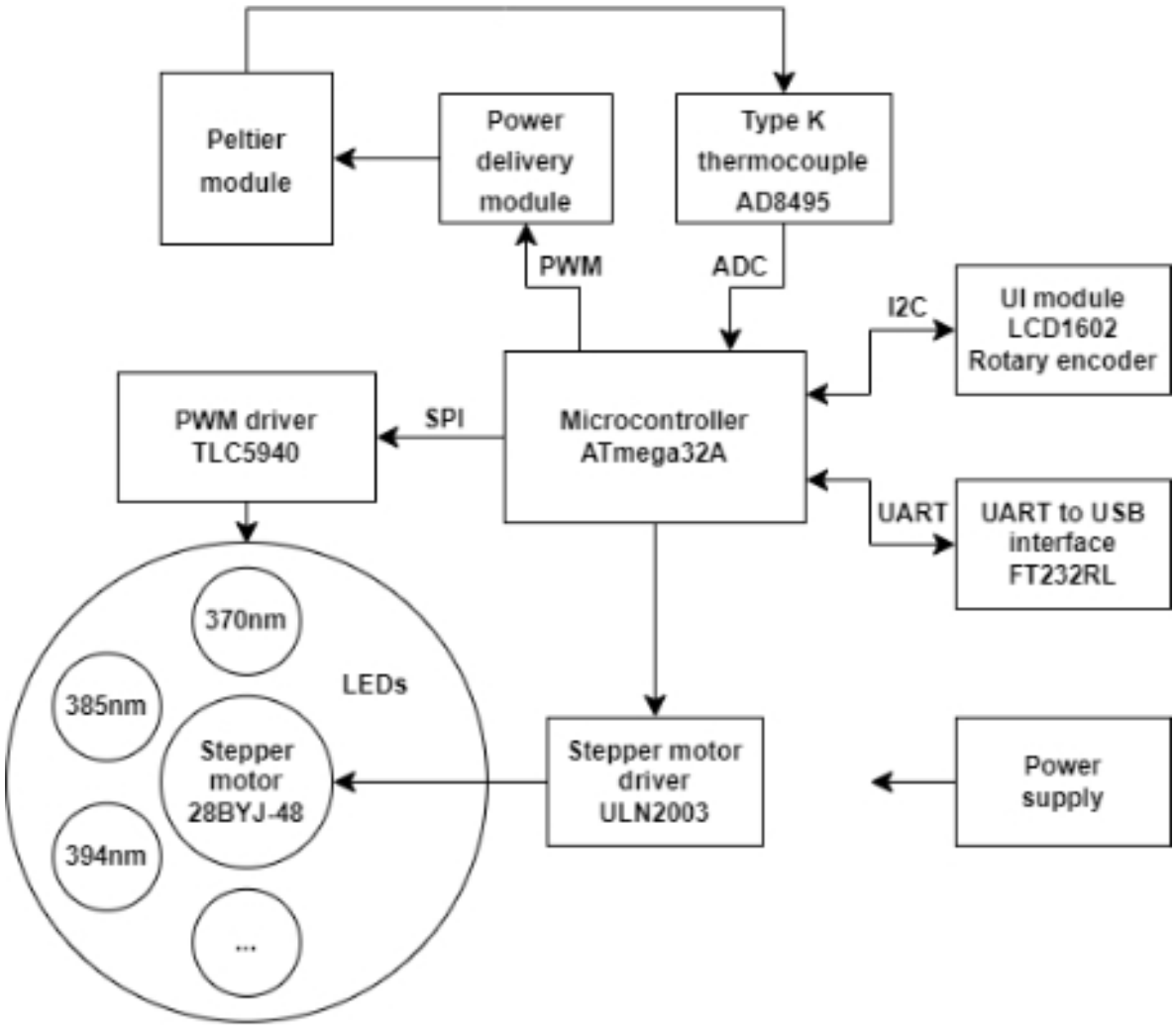

Figure 1. Schematic setup for testing the fabricated UV sensors at different regimes.

The light intensity of the LEDs is set via a PWM controller TLC5940, capable of setting the exact level of illumination the LED will provide. From minimum to maximum

value, we can have about 4000 different intensities. The working frequency of the PWM is about 2 kHz. The maximum current limit applied to the LED was 100 mA.

To study the response of the sample at different temperatures in the installation, a Peltier element is used. This element makes it possible to set the sample temperature in the range -10 to +100 °C. The Peltier element is controlled by a module which consists of a power MOSFET transistor and a relay with a double group of contacts. The transistor is driven with a PWM signal generated from the result of the proportional-integral-differential (PID) controller. The feedback signal for the PID, is acquired via a K-type thermocouple. The signal from this thermocouple is amplified via the AD8495 and applied to an ADC input of the microcontroller. Depending on the polarity of the voltage applied to the Peltier element, it will heat or cool the sample. The polarity change is done by using a relay with 2 groups of contacts.

Setting the wavelength, the applied light intensity and the temperature at which the measurement is made can be done in two ways. The first mode is the manual mode, the selection of the required parameters is done by means of the rotary encoder and the menu will be displayed on an LCD screen. The second mode involves connecting the measuring system to the computer via the USB port, this allows greater flexibility in generating UV radiation pulses. The measurement of the sample is taken in electrical current. Sample data being acquired via Keithley Model 2450 source meter. The entire configuration is supervised by special software. All baseline measurements were performed at a bias voltage of 1 V. In such a way it is possible to compare results.

3. Results and Discussion

The investigation of surface morphology and composition of ZnO:Al structures were analyzed by using SEM/EDX set-up. The SEM image of structural surface and morphology of ZnO:Al layer is as shown in Figure 2. It was observed uniform deposition on the glass substrate film of interconnected columnar grains, Figure 2. In some regions, interconnected columnar nanostructures form a flower-like (marked in red circle on Figure 2a morphology, most probably due to Al-doping and impurity segregation. Interconnected columnar grains have an advantage for sensing applications [24] due to an increased surface as adsorption sites. At higher magnification (Figure 2b) it was observed that columnar grain has rough surface which is another advantage for sensing applications, by increasing surface to volume ratio [24] and columns are interpenetrated and creates a huge number of potential barriers in between.

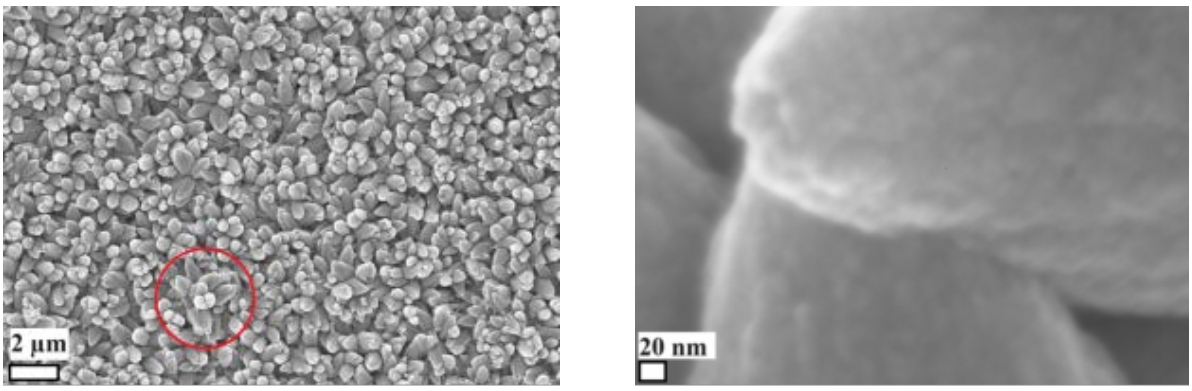

a) b)

Figure 2. SEM images of ZnO:Al structures at different scales: a) 2 µm; b) 20 nm showing columnar and interpenetrated nano- and micro-crystals.

For XRD measurements, $CuK_{\alpha 1}$ radiation source of Siefert 3000TT diffractometer was used with reflection geometry using PIXcel detector in 2θ range of 20° to 60° values were recorded. The XRD characterization carried out to study the crystallinity of ZnO:Al film used for developing sensors. It shows XRD pattern of film with multiple ZnO diffractions as $(10\bar{1}0)$, (0002), $(10\bar{1}1)$, $(10\bar{1}2)$, $(10\bar{2}0)$ at respective angles as shown in Figure 3. The major ZnO diffraction peak is (0002), at 34.3° with highest intensity showing a hexagonal structure and preferential growth along *c*-axis as already observed in our previous studies [24]. These reflexes can be attributed to PDF 036-1451 for ZnO and no alumina reflexes can be observed is ascribed as due to amorphous nature or much lower quantity of Al-related material vs ZnO, ZnO:Al film after thermal annealing at 625°C for 2 h and this can be attributed to PDF 00–004-0787.

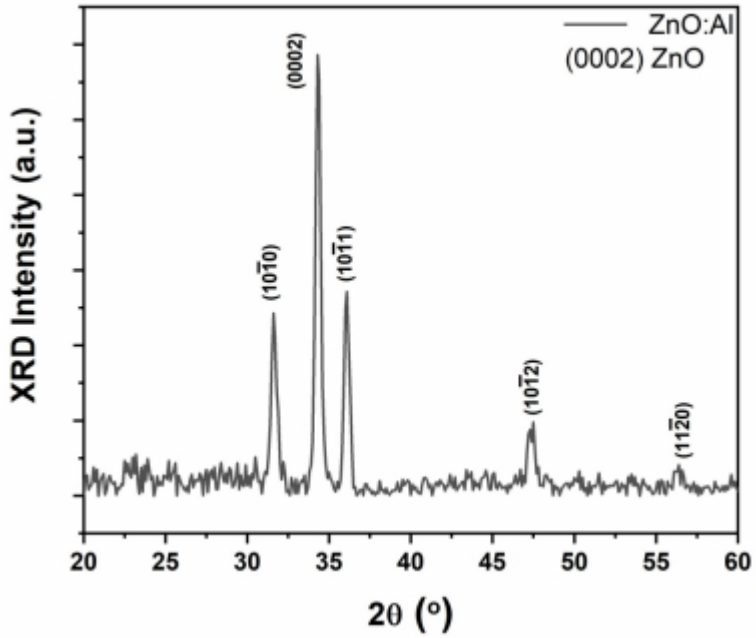

Figure 3. XRD pattern of studied ZnO:Al structure.

MicroRaman scattering investigations on developed samples were done at 22°C with a WITec LabRam Alpha 300 system in a backscattering configuration. The 532 nm laser was used for off-resonance excitation with less than 5 mW power at the specimen. Using optical objective lens placed on optical microscope, focusing of light was controlled on the sample surface. The CCD detector was used to collect photons and detect quickly the whole spectra.

To study the structural quality of these ZnO:Al layers on the substrate, detailed microRaman spectroscopy measurements at various locations in the specimen have been done. The absorption band edge of ZnO:Al layer was studied.

In figure 4(a) is presented micro-Raman spectra of ZnO:Al structure at room temperature, observing E_2(high)-E_2(low), A_1(TO) and E_2(high) modes at 330, 375 and 435 cm^{-1}, corresponding to wurtzite ZnO [24].

From Figure 4(b) we observed that E_2(high) mode is distributed uniformly, which indicates a high crystal quality of the film [24], as observed in SEM results. The clusters formed are characterized by sizes (Figure 2) and roughness (Figure 4b) corresponding to ZnO:Al made at low synthesis temperatures and not thermally treated one.

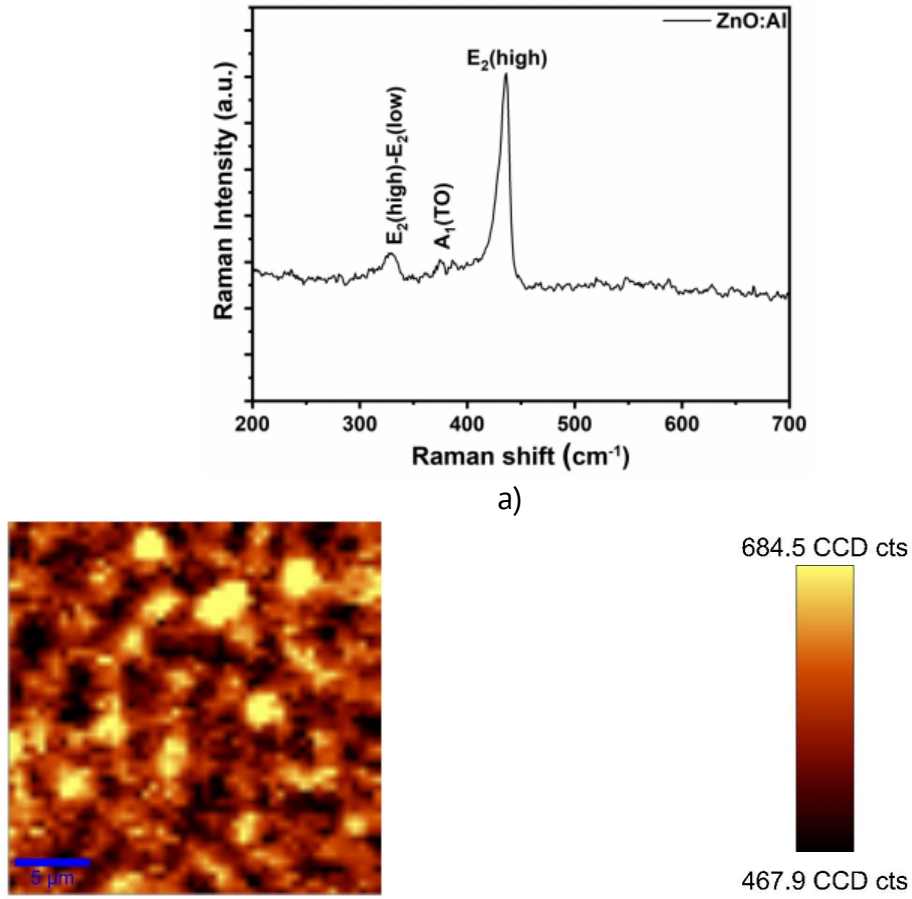

Figure 4. Micro-Raman spectra of ZnO:Al structure (a). Micro-Raman mapping of ZnO:Al structure (b).

When we talk about UV detectors, an important parameter is the dependence of their performance on working temperature. ZnO:Al structures presented in this research article exhibited a significant response at 370 nm wavelength at an operating temperature of 25 °C (Figure 5). The response of ZnO:Al to UV light can be explained by electronic and optical properties as shown in Figure 5. Al content in ZnO can deteriorates structural defects and enhances UV sensitivity [18] after thermal annealing.

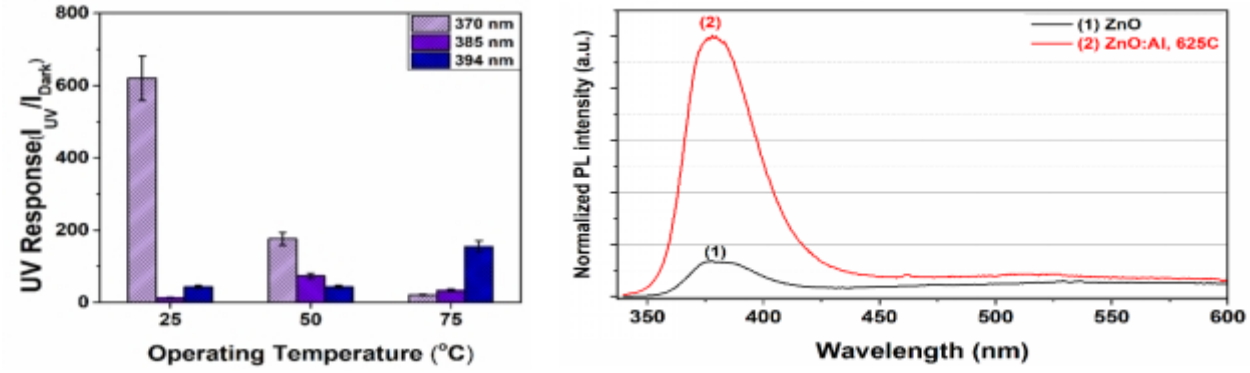

Figure 5. UV Response of ZnO:Al structures at different wavelengths versus operating temperature (a). Normalized photoluminescence of ZnO and annealed ZnO:Al at 625 °C (b).

Upon exposure to UV light, ZnO:Al structure shows a significant increase in photoconductivity attributed to enhancement in number of free charge carriers as a result of generation of electron–hole pairs by absorption of photons from UV light illumination (370 nm, 4.1 μW).

In absence of additional thermal annealing for sensor, its UV response for λ=370 nm monotonically decreases by increase in operating temperature from 25 °C to 75 °C (Figure 5a). This is due to cumulative effect resulting from bandgap changes, increase in crystal lattice scattering, increase in dark current with temperature caused by carrier thermogeneration, and favor of oxygen diffusion neutralizes some of the oxygen vacancies of ZnO caused by Al presence in ZnO matrix as reported previously [25]. Due to thermal annealing and Al diffusion onto the sensing surface of developed sensor, there is decrease in visible spectra luminescence related to lattice defects and increase in UV luminescence at about 370 nm (Figure 5b) could be considered as due to effective activation of Al diffusion after initial thermal annealing at 625°C for 2 h, confirmed in previous reports too [26]. Consequently, this contributes to excellent sensitivity of 370 nm over other higher wavelengths.

An increase in excitation wavelength (from 370 to 394 nm) leads to decrease in value of the UV response due to several competing factors (decreasing energy of absorbed photons, increasing absorption coefficient of material) [27].

Figure 5a shows UV response of such ZnO:Al structure-based sensor before thermal annealing (at 250 °C for 1 h) measured at operating temperature of 25 °C. At this temperature, we observed response of 620 at 370 nm wavelength, and response of 43 for the wavelengths 394 nm as shown in Table 1 for comparison. With increase in operating temperature of these nanostructures, a decrease in response to 370 nm wavelength is observed. Error bars in Figure 5a shows standard deviation in represented UV response value within 10% error.

Table 1

UV response before thermal annealing for ZnO:Al structures at different UV wavelengths. Operating temperatures of T= 25 °C, 50 °C, and 75 °C.

Temperature	UV Response, λ=370 nm	UV Response, λ=385 nm	UV Response, λ= 394 nm
25 °C	~620	~13	~43
50 °C	~176	~73.5	~43.4
75 °C	~22	~34	~155

Thus, before thermal annealing of sensor (at 250 °C for 1 h) measured at low operating temperature of 25 °C, wavelength of 370 nm is considered as optimal ascribed as due to ZnO:Al energy bandgap (~3.35 eV) correspondence to optimal wavelength as shown in Eq. (1).

$$EQE, \eta = \frac{hcR}{\lambda q} \quad (1)$$

Response and fall times of the ZnO:Al structures for the wavelength 370 nm at operating temperature of 25 °C is as shown in Figure 6. Response/fall time is defined as time taken to achieve 90%/10% of its maximum response value, respectively. We note that response time is approximately 39 seconds and the fall time 4109 seconds for 25 °C operating temperature.

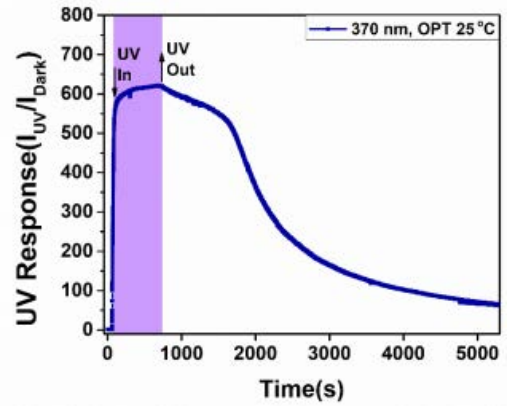

Figure 6. Dynamic UV response of ZnO:Al structure-based sensor measured under UV radiation (370 nm) before thermal annealing of the sample. The operating temperature is 25 °C.

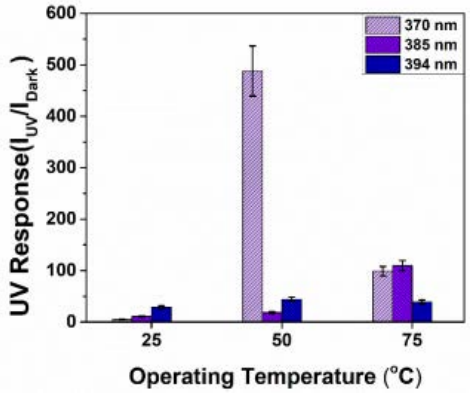

Figure 7. UV response of ZnO:Al structure-based sensor vs operating temperature. The sensor structure was thermally annealed at T_{ann} = 250 °C for 1 hour in air and measured at temperatures of 25, 50 and 75 °C, respectively. UV excitation was 370, 385 or 394 nm, respectively.

Figure 7 shows the UV response of ZnO:Al structure-based sensor after thermal annealing (at 250 °C for 1 h) and measured at operating temperatures of 25 °C, 50 °C, and 75 °C. Error bars in Figure 7 has standard deviation in represented UV response value with 10% error.

Data processing tells us (Table 2) that at operating temperature of 25 °C, we observed response of ~4.7, ~10.8 and ~28.7 for the wavelengths 370 nm, 385 nm and 394 nm, respectively. It was observed that at working temperature of 50 °C for 370 nm UV illumination device exhibits response of ~488 which is about 102 times higher than at other tested wavelengths, where relatively lower response values of approximately ~18.3 and ~43.8, respectively. After thermal annealing of sensor structure, it was observed that UV response at 75 °C comes out to be ~99, ~109 and ~39 for 370 nm, 385 nm, and 394 nm wavelengths, respectively. Thus, after thermal annealing maximum response at operating temperature of 50 °C for optimal wavelength 370 nm was observed as ~488.

Table 2

UV response for ZnO:Al -based sensor after thermal annealing investigated at different UV wavelengths and measurement temperatures (25 °C, 50 °C and 75 °C).

Temperature	UV Response, λ=370 nm	UV Response, λ=385 nm	UV Response, λ=394 nm
25 °C	~4.7	~10.8	~28.7
50 °C	~488	~18.3	~43.8
75 °C	~99	~109.4	~39

Figure 8 shows the dynamic response of ZnO:Al -based sensor after thermal annealing (at regime 250 °C for 1 h). The thermal annealing of entire sensor exhibits excellent improvement in its fall rate and UV response for 370 nm illumination as compared to sample before thermal annealing and measured at operating temperature of 50 °C. UV response increased from 176 to about 488 and the fall time reduces to 449 seconds as shown in Figures 5, 7 and 10, respectively.

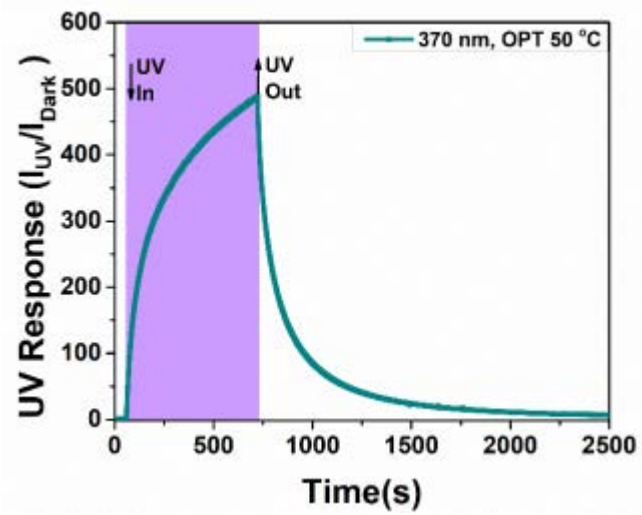

Figure 8. UV Dynamic response of ZnO:Al sensor after thermal annealing and investigated at radiation wavelength of 370 nm and operating temperature of 50 °C.

The dynamic response of the ZnO:Al sensor after thermal annealing and investigated for the different applied bias voltages as show in Figure 9. It was observed for applied bias voltage of 0.1 V (Figure 9 (curve 1)) rise time and fall time of approximately 325 seconds and 306 seconds, respectively. At an applied bias voltage of 0.5 V (Figure 9 (curve 2)), we obtained rise time of 449 seconds and fall time of about 585 seconds for this sample. At an applied bias voltage of 1 V, we measured response time of 449 seconds and fall time of 448 seconds, observed in Figure 9 (curve 3). When applying bias voltage of 5 V observed in Figure 9 (curve 4), the response time is 485 seconds, and the fall time is 738 seconds. From Figure 9, it can be concluded that at an applied bias voltage of 0.5 V and 1 V response time is almost identical, while fall time differs by about 140 seconds. Applying bias voltage of 5 V increases the fall time significantly by a ratio of about 1.6 times, but a response time remains same.

UV response analysis of semiconductor material is a complex process. It depends upon lot of operating parameters that can be controlled to optimize desired UV response at appropriate conditions. Under influence of applied bias voltage and UV illumination, electron-hole pairs generation and recombination may occur. For ZnO:Al -based sensor structures transient properties of UV detection influenced by applied bias voltage as given by E=V/L, where E, V, and L represents applied electric field due to bias voltage, potential difference between electrodes, and distance between electrodes, respectively.

By increase in applied bias voltage, electric field across sensing electrodes increases. Hence stronger charge carrier separation ability, large amount of photo generated charge carriers and fall time increases at higher bias voltage [15].

$$I_{ph} = \frac{q.\Phi.n.\tau_{carrier}}{\tau_{transit}} \tag{2}$$

where:

$$\tau_{transit} = \frac{l^2}{\mu V} \tag{3}$$

where: I_{ph}, $\tau_{transit}$, Φ, n, $\tau_{carrier}$, μ, l, and V represents UV current, transit time across sensor active region, number of photons incident on sensing surface per second, absorption

quantum efficiency, carrier life time, mobility of charge carriers, length of electrode, and bias voltage, respectively.

By increasing applied voltage UV current also increases from Eq. (2) and (3) [28]. Hence, UV response increases by increase in applied bias voltage.

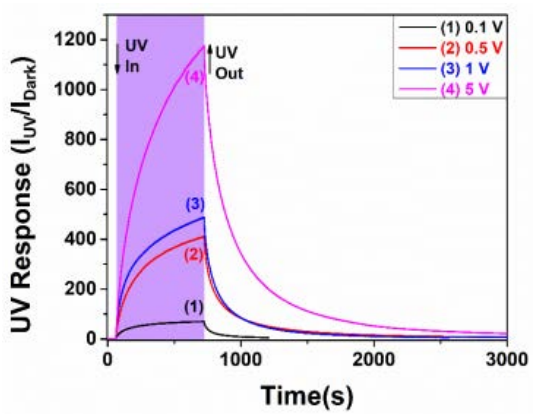

Figure 9. UV Dynamic response of ZnO:Al-based sensor after thermal annealing and investigated at radiation wavelength of 370 nm and operating temperature of 50 °C. Applied bias voltages were (1) 0.1 V; (2) 0.5 V; (3) 1 V; and (4) 5 V, respectively.

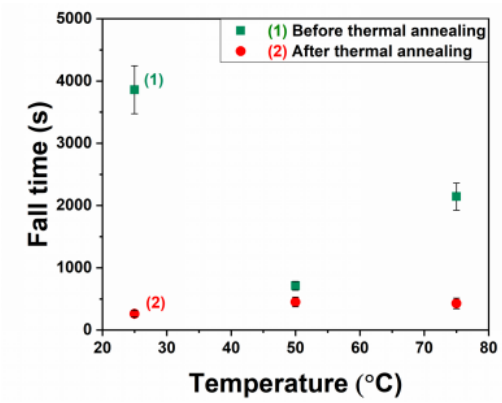

Figure 10. Effect of thermal annealing of sensor structure on its fall time versus operating temperature under UV irradiation.

Effect of thermal annealing on fall time for ZnO:Al -based sensor after thermal annealing can be seen in Figure 10. The thermal annealing of sensor structure at a temperature of 250 °C for 1 h improves the UV fall and enhances the fall rate for UV illumination at optimal conditions i.e. 370 nm as shown in Figure 10. This may be due to faster evacuation/extraction of electrical charge carries. The error bars in Figure 10 has standard deviation in represented fall time value with 10% error. Before thermal annealing, UV decay rate after UV inactivation was slow especially at operating temperature of 25 °C, but after thermal annealing decay rate becomes fast enough irrespective of operating temperature [29]. After annealing, elimination of deep trap states enhances the surface quality and increases the recovery rate [30].

Thermal effect on sensor structure effectively contributes to conductivity of material and enhances current contribution to the sensing surface. By increasing operating temperature, more electrons reach to the conduction band which leads to increase in carrier concentration. Consequently, it enhances conductivity and current on the sensing surface. This can be understood well with the help of following two relations [31]:

$$\sigma = ne\mu_e \tag{4}$$

$$n = \sqrt{N_D N_C}.\left(\frac{2\pi m_e kT}{h^2}\right)^{\frac{3}{2}}.\exp\left(-\left(\frac{E_C - E_D}{2kT}\right)\right) \tag{5}$$

where: σ represents electrical conductivity at given temperature, n is intrinsic carrier concentration, μ_e is electron mobility, N_D represents density of donor states, N_C represents density of states in conduction band, m_e represents effective mass of electron, E_C and E_D represents bottom edge energy of conduction band and donor level energy, respectively.

Figure 11 can be ascribed by Eq. (4) and (5). As it shows, carrier concentration increases by increase in temperature which leads to the increase in electrical conductivity (or current). Since, oxide semiconductor has negative temperature coefficient of resistance. Thus, current increases by increase in operating temperature.

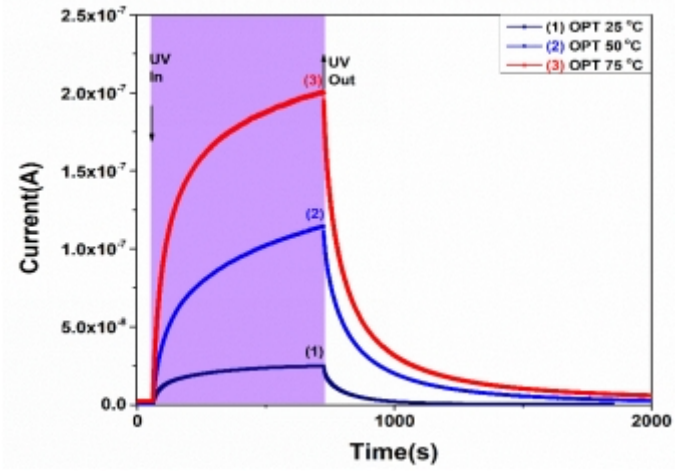

Figure 11. Effect of operating temperature on electrical current as a function of time (dynamic responses) for ZnO:Al -based sensor after thermal annealing and investigated at different operating temperatures.

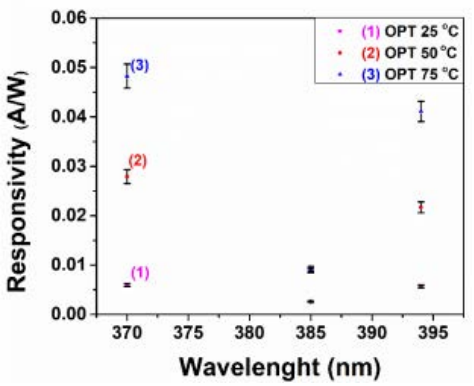

Figure 12. Responsivity of ZnO:Al -based sensor after thermal annealing and investigated at different operating temperature *vs* UV wavelengths of applied radiation.

Maximum responsivity at 370 nm is ascribed as due to energy bandgap correspondence of ZnO:Al to ~370 nm wavelength. Due to presence of Al in ZnO microparticles, high temperature annealing (625 °C, 2 h) provides more activation energy influences Al^{3+} ions and allows diffusion of Al^{3+} into the sample through interstitial mechanism which leads to excellent sensitivity [32]. In Figure 12, 385 nm and 394 nm peaks are accounted for acceptor bound exciton and free electron to acceptor emission [33], respectively.

After thermal treatment, UV responsivity comes out to be maximum for optimal wavelength 370 nm at operating temperature of 75 °C as shown in Figure 12. Error bars in Figure 12 has standard deviation in represented responsivity value with 10% error.

$$\sigma = \sigma_0 e^{\frac{-E_a}{k_B T}} \tag{6}$$

where: σ, σ_o, E_a, k_B, and T represents conductivity at given temperature, conductivity at absolute temperature, activation energy, Boltzmann constant, and operating temperature, respectively.

By increasing temperature, conductivity increases as shown in Eq. (6) [34]. Thus, it contributes to carrier concentration and hence responsivity enhances as shown in Eq. (7):

$$Responsivity = \frac{(I_{UV} - I_{dark})(for\ given\ \lambda)}{P(for\ given\ \lambda)}, \left(\frac{A}{W}\right) \tag{7}$$

where: I_{UV}, and I_{dark} represents UV current and dark current respectively (A), P represents optical power for each wavelength (Watt).

External quantum efficiency calculated for all three wavelengths as shown in Eq. (8) and it comes out to be maximum for 370 nm at operating temperature of 75 °C as 0.16 which is eight to ten times higher than at other tested UV-wavelength, i.e. 385 nm.

$$EQE, \eta = \frac{hcR}{\lambda q} \tag{8}$$

where: η is external quantum efficiency, λ is illuminated wavelength, q is carrier charge, h is Planck's constant, c is speed of light, and R is responsivity.

Table 3 shows calculated of Responsivity R and external quantum efficiency at three different UV wavelengths used in this work and as shown below.

Table 3

Responsivity and external quantum efficiency of ZnO:Al structure-based sensor after thermal annealing measured at three different UV wavelengths. Operating temperatures were (25 °C, 50 °C and 75 °C).

Wavelength, nm	Responsivity, 25 °C	Responsivity, 50 °C	Responsivity, 75 °C	EQE, 25°C	EQE, 50°C	EQE, 75°C
370	0.006	0.027	0.048	0.020	0.090	0.160
385	0.002	0.008	0.009	0.006	0.025	0.028
400	0.005	0.021	0.041	0.015	0.065	0.127

A sensing mechanism proposed for investigated sensors

By increase in temperature, dark current increases exponentially as described by Arrhenius Eq. (9) [16]

$$I_d = A.I_{d_o}.exp\left(-\frac{E_a}{k_B T}\right) \tag{9}$$

where: A is proportionality constant, k_B is Boltzmann constant, E_a is activation energy, I_{d0} is preexponential factor and T is the operating temperature.

According to the results from Figure 5a, optimal wavelength comes out to be 370 nm which exhibits maximum response as 620 among all other UV-A wavelengths ascribed as due to the energy band gap correspondence to 370 nm wavelength for ZnO:Al at operating temperature of 25 °C. From PL spectra, 370 nm peak can be attributed to the localized bound exciton emission at longer wavelength caused by the Al diffusion on ZnO sensing surface [35]. Due to the presence of Al, this peak blue shifted to 370 nm. SEM image in Figure 2b shows rough surface due to presence of Al in ZnO leads to absorption of 370 nm UV irradiation and enhancement in sensitivity towards UV range near to its band gap energy correspondence [36,37].

Due to UV illumination at 370 nm wavelength ensure electron-hole pairs generated after photon absorption as shown in Eq. (10).

$$h\nu \rightarrow e^- + h^+, \tag{10}$$

where h, ν, e^-, and h^+, are Planck's constant, frequency of illuminated radiation, photogenerated electron and hole, respectively.

UV absorption not only contributes to electron-hole pairs generation but also leads to chemisorption of oxygen molecule and their surface kinetics reactions with generated electron-hole pair as shown in Eq. (11) and (12):

$$O_{2(gas)} + e^- \rightarrow O_{2\ (ads.)}^- \quad (11)$$

$$O_{2(ads.)}^- + h^+ \rightarrow O_{2(desorp.)}, \quad (12)$$

where: $O_{2(gas)}^-$, $O_{2(ads.)}^-$ and $O_{2(desorp.)}$ represents oxygen gas molecule, adsorbed oxygen ion and desorbed oxygen molecule, respectively.

The surface charge carriers' kinetics vary by UV illumination. In an ambient environment, oxygen gaseous molecules react with free electrons and get adsorbed on sensing surface as shown in Eq. (11) which leads to decrease in electrical conductivity of ZnO networks. This is due to *n*-type character of ZnO networks in which electrons are the majority charge carriers which contributes to the conduction process. Under UV illumination ($h\nu > E_g$), a photogenerated electron-hole pair occurs as shown in Equation 10 where photogenerated electrons contribute to the enhancement in electrical conductivity and photogenerated holes also reacts with adsorbed oxygen ions as shown in Eq. (12). Finally, this process leads to the desorption of oxygen from the sensor surface.

Diffusion of Al in ZnO (which anyway has many defects (oxygen vacancies)) additionally forms electrons that reduce the amount of O_2 by reducing it to ion forms, especially to the form of superoxide O_2^-. Increasing the concentration of such oxygen radicals increases the catalytic reactions of the ZnO:Al surface, additionally amplified by UV irradiation. This overall leads to an increase in the sensitivity of the sensor to UV spectra. This can be confirmed through SEM and PL spectra results as shown in Figure 2b, 4a, and 5b, respectively.

Figure 13 shows general UV sensing mechanism proposed for such ZnO:Al structures. Eq. (11) and (12) elucidates this UV sensing mechanism in equation form. As Eq. (11) demonstrates reaction of free electrons with oxygen gas present in atmosphere and transition from initial stage represented in Figure 13a to stage represented in Figure 13b. Next, Eq. (12) demonstrates adsorbed oxygen reaction with photogenerated holes which leads to the oxygen desorption and transition from stage represented in Figure 13c to stage represented in Figure 13d after UV illumination on the sensing surface of the sensor.

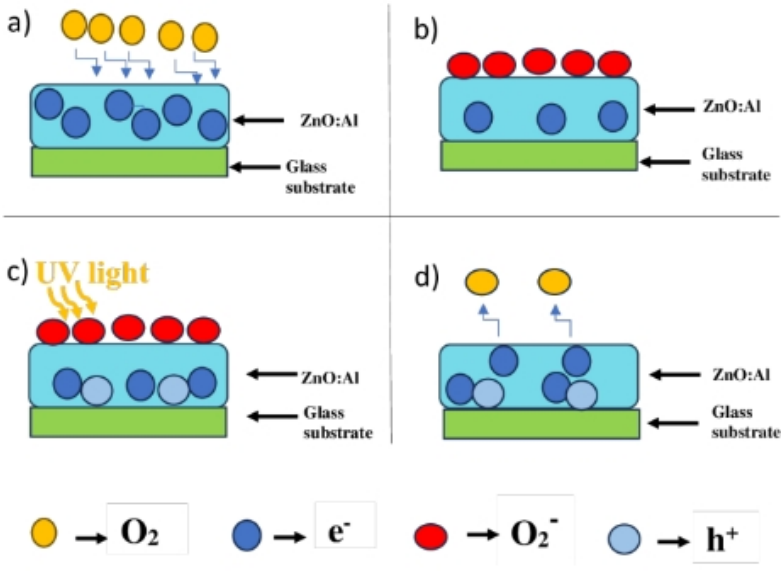

Figure 13. Schematic representation of UV sensing mechanism proposed in four stages: a) Initial stage without oxygen adsorption; b) oxygen adsorption; c) UV excitation; d) oxygen desorption.

5. Conclusions

Although UV radiation is a form of non-ionizing radiation, its presence in nature (10% of solar UV radiation penetrates the atmosphere and reaches the Earth's surface), in multiple industrial processes, in specific applications like (tanning bed, mercury vapor lighting in stadiums, school gyms, some halogen, fluorescent and incandescent lights, some types of lasers, etc.) is a serious reason for ensuring effective monitoring of exposure to UV radiation. It is important to remember that in 2009 the WHO declared UV radiation as completely carcinogenic, as it is both a mutagen and non-specific damaging agent and it plays a role in both initiating and promoting tumors.

Due to the need to control the presence and level of ionizing radiation, multiple researches are initiated, including the development of new sensors based on semiconductor structures such as ZnO doped with Al. The results obtained and presented in the research of the ZnO:Al structure as UV radiation sensors can be concluded by the following.

ZnO:Al structures not subjected to thermal treatment are promising as sensors for UV detection at room temperature. Their thermal treatment leads to an increase in their working temperature. Thus, depending on the operating conditions, the same structures by simple thermal annealing change the optimal operating temperature, thus ensuring a selectivity of the sensor.

The PL spectra denote the effect of Al doping and thermal annealing on enhancement of UV intensity and removing of visible ranged defects.

Increasing the applied bias voltage provides an improvement in the UV response current for the optimal wavelength of 370 nm.

Thermal annealing leads to a remarkable improvement in fall response time irrespective of operating temperature for thermally annealed sensors. An increase in temperature causes an increase in current which can be ascribed as due to the thermal contribution to current and hence, conductivity of ZnO:Al structure. Overall, maximal responsivity is demonstrated by UV irradiation with optimal wavelength of 370 nm which is about ten times higher as compared to another interfering wavelength of 385 nm at 75 °C. This study exhibits excellent UV response at room temperature and at higher temperatures even with low optical illumination of 4.1 μW and relatively low applied bias voltage of 1 V which elucidates its excellence for range of photodetection applications. A mechanism is also presented that explains the sensitivity of the ZnO:Al structure to UV radiation in different operating conditions.

The monitoring of UV rays is one of the necessary criteria to limit its adverse impact on human health at the level of the natural rays emitted by the sun as well as the artificial ones emitted by various domestic and industrial devices used in working conditions.

Acknowledgments: This paper was supported by the project EU-project SENNET "Porous Networks for Gas Sensing", which runs under the Marie Sklodowska-Curie Actions funded by the European Union, under the number 101072845.

Conflicts of Interest: The authors declare no conflict of interest.

References

1. Giannos, S.A.; Kraft, E.R.; Lyons, L.J.; Gupta, P.K. Spectral Evaluation of Eyeglass Blocking Efficiency of Ultraviolet/High-Energy Visible Blue Light for Ocular Protection. *Optometry and vision science : official publication of the American Academy of Optometry* 2019, 96, pp. 513–522, doi:10.1097/OPX.0000000000001393.

2. Kraemer, K.H.; Lee, M.M.; Scotto, J. Xeroderma Pigmentosum. Cutaneous, Ocular, and Neurologic Abnormalities in 830 Published Cases. *Archives of dermatology* 1987, 123, pp. 241–250, doi:10.1001/archderm.123.2.241.
3. Wang, X.; Tao, P.; Wang, Q.; Zhao, R.; Liu, T.; Hu, Y.; Hu, Z.; Wang, Y.; Wang, J.; Tang, Y.; et al. Trends in Photoresist Materials for Extreme Ultraviolet Lithography: A Review. *Materials Today* 2023, 67, pp. 299–319, doi:https://doi.org/10.1016/j.mattod.2023.05.027.
4. Al Qahtani, M.S.A.; Wu, Y.; Spintzyk, S.; Krieg, P.; Killinger, A.; Schweizer, E.; Stephan, I.; Scheideler, L.; Geis-Gerstorfer, J.; Rupp, F. UV-A and UV-C Light Induced Hydrophilization of Dental Implants. *Dental Materials* 2015, 31, pp. e157–e167, doi:https://doi.org/10.1016/j.dental.2015.04.011.
5. Hiroko Inagaki Akatsuki Saito, H.S.T.O.; Fujimoto, S. Rapid Inactivation of SARS-CoV-2 with Deep-UV LED Irradiation. *Emerging Microbes \& Infections* 2020, 9, pp. 1744–1747, doi:10.1080/22221751.2020.1796529.
6. Lupan, O.; Postica, V.; Wolff, N.; Polonskyi, O.; Duppel, V.; Kaidas, V.; Lazari, E.; Ababii, N.; Faupel, F.; Kienle, L. Localized Synthesis of Iron Oxide Nanowires and Fabrication of High Performance Nanosensors Based on a Single Fe2O3 Nanowire. *Small* 2017, 13, 1602868, doi:https://doi.org/10.1002/smll.201602868.
7. Barros, N. de M.; Sbroglio, L.L.; Buffara, M. de O.; Baka, J.L.C.E.S.; Pessoa, A. de S.; Azulay-Abulafia, L. Phototherapy. *Anais brasileiros de dermatologia* 2021, 96, pp. 397–407, doi:10.1016/j.abd.2021.03.001.
8. Koutchma, T. UV Light for Processing Foods. *Ozone: Science & Engineering* 2008, 30, pp. 93–98, doi:10.1080/01919510701816346.
9. Brinza, M.; Schröder, S.; Ababii, N.; Gronenberg, M.; Strunskus, T.; Pauporte, T.; Adelung, R.; Faupel, F.; Lupan, O. Two-in-One Sensor Based on PV4D4-Coated TiO2 Films for Food Spoilage Detection and as a Breath Marker for Several Diseases. *Biosensors* 2023, 13, 538, doi:10.3390/bios13050538.
10. Ju, J.-H.; Yoon, Y.-H.; Shin, S.-H.; Ju, S.-Y.; Yeum, K.-J. Recent Trends in Urban Agriculture to Improve Bioactive Content of Plant Foods. *Horticulturae* 2022, 8(9), 767 doi:10.3390/horticulturae8090767.
11. Dinani, N.; George, S. Nail Cosmetics: A Dermatological Perspective. *Clinical and Experimental Dermatology* 2019, 44, pp. 599–605, doi:10.1111/ced.13929.
12. Berardesca, E.; Zuberbier, T.; Sanchez Viera, M.; Marinovich, M. Review of the Safety of Octocrylene Used as an Ultraviolet Filter in Cosmetics. *Journal of the European Academy of Dermatology and Venereology* 2019, 33, pp. 25–33, doi:https://doi.org/10.1111/jdv.15945.
13. Huang, X.; Chalmers, A.N. Review of Wearable and Portable Sensors for Monitoring Personal Solar UV Exposure. *Annals of Biomedical Engineering* 2021, 49, pp. 964–978, doi:10.1007/s10439-020-02710-x.
14. Engelsen, O. The Relationship between Ultraviolet Radiation Exposure and Vitamin D Status. *Nutrients* 2010, 2, pp. 482–495, doi:10.3390/nu2050482.
15. Zhou, X.; Jiang, D.; Yang, X.; Duan, Y.; Zhang, W.; Zhao, M.; Liang, Q.; Gao, S.; Hou, J.; Zheng, T. Voltage-Dependent Responsivity of ZnO Schottky UV Photodetectors with Different Electrode Spacings. *Sensors and Actuators A: Physical* 2018, 284, pp. 12–16, doi:https://doi.org/10.1016/j.sna.2018.09.032.
16. Lu, H.F.; Fu, L.; Jolley, G.; Tan, H.H.; Tatavarti, S.R.; Jagadish, C. Temperature Dependence of Dark Current Properties of InGaAs/GaAs Quantum Dot Solar Cells. *Applied Physics Letters* 2011, 98, 183509, doi:10.1063/1.3586251.
17. Azizah, N.; Muhammady, S.; Purbayanto, M.A.K.; Nurfani, E.; Winata, T.; Sustini, E.; Widita, R.; Darma, Y. Influence of Al Doping on the Crystal Structure, Optical Properties, and Photodetecting Performance of ZnO Film. *Progress in Natural Science: Materials International* 2020, 30, pp. 28–34, doi:https://doi.org/10.1016/j.pnsc.2020.01.006.
18. Pradhan, P.; Alonso, J.C.; Bizarro, M. Photocatalytic Performance of ZnO: Al Films under Different Light Sources. *International Journal of Photoenergy* 2012, 2012, 780462, doi:10.1155/2012/780462.
19. Chakraborty, B.; Schadte, P.; Poschmann, M.P.M.; Lupan, C.; Zadorojneac, T.; Magariu, N.; Padunnappattu, A.; Schütt, F.; Lupan, O.; Siebert, L. MOF-Coated 3D-Printed ZnO Tetrapods as a Two-in-One Sensor for H2 Sensing and UV Detection. In: *Proceedings of the 6th International Conference on Nanotechnologies and Biomedical Engineering*; Sontea, V., Tiginyanu, I., Railean, S., Eds.; Springer Nature Switzerland: Cham, 2024, pp. 70–79.
20. Lupan, O.; Santos-Carballal, D.; Magariu, N.; Mishra, A.K.; Ababii, N.; Krüger, H.; Wolff, N.; Vahl, A.; Bodduluri, M.T.; Kohlmann, N. Al2O3/ZnO Heterostructure-Based Sensors for Volatile Organic Compounds in Safety Applications. *ACS Applied Materials & Interfaces* 2022, 14, pp. 29331–29344, doi:10.1021/acsami.2c03704.
21. Lupan, O.; Shishiyanu, S.; Chow, L.; Shishiyanu, T. Nanostructured Zinc Oxide Gas Sensors by Successive Ionic Layer Adsorption and Reaction Method and Rapid Photothermal Processing. *Thin Solid Films* 2008,

516, pp. 3338–3345, doi:https://doi.org/10.1016/j.tsf.2007.10.104.
22. Lupan, O.; Chow, L.; Shishiyanu, S.; Monaico, E.; Shishiyanu, T.; Şontea, V.; Roldan Cuenya, B.; Naitabdi, A.; Park, S.; Schulte, A. Nanostructured Zinc Oxide Films Synthesized by Successive Chemical Solution Deposition for Gas Sensor Applications. *Materials Research Bulletin* 2009, 44, pp. 63–69, doi:https://doi.org/10.1016/j.materresbull.2008.04.006.
23. Lupan, O.; Ababii, N.; Mishra, A.K.; Bodduluri, M.T.; Magariu, N.; Vahl, A.; Krüger, H.; Wagner, B.; Faupel, F.; Adelung, R.; et al. Heterostructure-Based Devices with Enhanced Humidity Stability for H2 Gas Sensing Applications in Breath Tests and Portable Batteries. *Sensors and Actuators A: Physical* 2021, 329, 112804, doi:https://doi.org/10.1016/j.sna.2021.112804.
24. Hoppe, M.; Ababii, N.; Postica, V.; Lupan, O.; Polonskyi, O.; Schütt, F.; Kaps, S.; Sukhodub, L.F.; Sontea, V.; Strunskus, T.; et al. Sensors and Actuators B : Chemical (CuO-Cu 2 O)/ ZnO : Al Heterojunctions for Volatile Organic Compound Detection. 2018, 255, pp. 1362–1375.
25. Pon, V.D.; Wilson, K.S.J.; Hariprasad, K.; Ganesh, V.; Ali, H.E.; Algarni, H.; Yahia, I.S. Superlattices and Microstructures Enhancement of Optoelectronic Properties of ZnO Thin Films by Al Doping for Photodetector Applications. *Superlattices and Microstructures* 2021, 151, 106790, doi:10.1016/j.spmi.2020.106790.
26. Shishiyanu, S.T.; Lupan, O.I.; Monaico, E. V; Ursaki, V. V; Shishiyanu, T.S.; Tiginyanu, I.M. Photoluminescence of Chemical Bath Deposited ZnO : Al Films Treated by Rapid Thermal Annealing. 2005, 488, pp. 15–19, doi:10.1016/j.tsf.2005.04.004.
27. Xie, Q.; Liu, X.; Liu, H. Fastly Steady UV Response Feature of Mn-Doped ZnO Thin Films. *Superlattices and Microstructures* 2020, 139, 106391, doi:https://doi.org/10.1016/j.spmi.2020.106391.
28. Wang, R.; Yang, L.; Xu, S.; Zhang, X.; Dong, X.; Zhao, Y.; Fu, K.; Zhang, B.; Yang, H. Bias-Voltage Dependent Ultraviolet Photodetectors Prepared by GaOx+ZnO Mixture Phase Nanocrystalline Thin Films. *Journal of Alloys and Compounds* 2013, 566, pp. 201–205, doi:https://doi.org/10.1016/j.jallcom.2013.03.039.
29. Kim, D.; Leem, J.-Y. Improving of the Rise and Decay Rates of an Ultraviolet Photodetector Using Stepwise Annealed ZnO Nanorods. *physica status solidi (a)* 2019, 216, 1800929, doi:https://doi.org/10.1002/pssa.201800929.
30. Thahe, A.A.; Ali, B.A.; Bakhtiar, H.; Uday, M.B.; Hassan, Z.; Abdullah, M.; Qaeed, M.A.; Alqaraghuli, H.; Zaidan, H.A.; Allam, N.K. Laser Annealing Enhanced the Photophysical Performance of Pt/n-PSi/ZnO/Pt-Based Photodetectors. *Solid-State Electronics* 2020, 171, 107821, doi:https://doi.org/10.1016/j.sse.2020.107821.
31. Li, P.; Meng, X. Thermal Annealing Effects on the Optoelectronic Characteristics of Fully Nanowire-Based UV Detector. *Journal of Materials Science: Materials in Electronics* 2016, 27, pp. 7693–7698, doi:10.1007/s10854-016-4755-3.
32. Wu, J.; Zhao, Y.; Zhao, C.Z.; Yang, L.; Lu, Q.; Zhang, Q.; Smith, J.; Zhao, Y. Effects of Rapid Thermal Annealing on the Structural, Electrical, and Optical Properties of Zr-Doped ZnO Thin Films Grown by Atomic Layer Deposition. *Materials* 2016, 9(8), 695 doi:10.3390/ma9080695.
33. Loughin, S.; French, R.; Noyer, L.; Ching, W.-Y.; Xu, Y.-N. Critical Point Analysis of the Interband Transition Strength of Electrons. *Journal of Physics D: Applied Physics* 1999, 29, 1740, doi:10.1088/0022-3727/29/7/009.
34. Srivastava, R. Investigation on Temperature Sensing of Nanostructured Zinc Oxide Synthesized via Oxalate Route. 2012, 2012, pp. 8–12.
35. Kshirsagar, S.; V V, N.; Mahamuni, S. Exciton Structure in Sodium Doped Zinc Oxide Quantum Dots. *Applied Physics Letters* 2006, 89, 53120, doi:10.1063/1.2222334.
36. Hamby, D.W.; Lucca, D.A.; Klopfstein, M.J. Photoluminescence of Mechanically Polished ZnO. *Journal of Applied Physics* 2005, 97, 43504, doi:10.1063/1.1840102.
37. Meyer, B.K.; Alves, H.; Hofmann, D.M.; Kriegseis, W.; Forster, D.; Bertram, F.; Christen, J.; Hoffmann, A.; Straßburg, M.; Dworzak, M. Bound Exciton and Donor–Acceptor Pair Recombinations in ZnO. *physica status solidi (b)* 2004, 241, pp. 231–260, doi:https://doi.org/10.1002/pssb.200301962.

Citation: Nagpal, R.; Chiriac, M.; Sereacov, A.; Birnaz, A.; Ababii, N.; Lupan, C.; Buzdugan, A.; Sandu, Iu.; Siebert, L.; Pauporté, T.; Lupan, O. Annealing effect on UV detection properties of ZnO:Al structures. *Journal of Engineering Science* 2023, 30 (4), pp. 45-62. https://doi.org/10.52326/jes.utm.2023.30(4).04.

Submission of manuscripts: jes@meridian.utm.md